

Supporting Information

Rietveld refinement details ($\text{Mg}(\text{BH}_4)_2 \cdot 3\text{N}_2\text{H}_4$ as an example):

The XRD pattern of $\text{Mg}(\text{BH}_4)_2 \cdot 3\text{N}_2\text{H}_4$ was indexed to a trigonal structure with lattice parameters of approximately $a=13.876 \text{ \AA}$ and $c=7.833 \text{ \AA}$. Assessment of the extinction symbol associated with the space group of the new phase indicated the most probable to be $P\bar{3}1c$. The crystal structure was then partially solved using direct methods under this space group. Due to the uncertain H positions, First-principles molecular dynamics simulated annealing were then performed to confirm the BH_4^- and N_2H_4 configuration with the lowest energy. Rietveld structural refinement on the optimal structural candidate was performed using the GSAS package [1] on the XRD data. The BH_4^- and N_2H_4 groups were kept as rigid bodies with common refined bond lengths and bond angles constrained as reasonable values due to the inadequate number of observations. These rigid bodies and the lattice parameters were refined, yielding the agreement factors of $R_{\text{wp}}=0.0285$, $R_{\text{p}}=0.0220$ and $R_{\text{F}2}=0.0712$. The Rietveld fit to the XRD pattern is shown in Figure 3.

The isotropic thermal parameters (U_{iso}) were constrained to be identical for the same rigid body type: $U_{\text{Mg}}=2.4(1)$, $U_{\text{BH}_4}=1.0(4)$, and $U_{\text{NH}_2\text{NH}_2}=1.9(7)$ ($\times 100 \text{ \AA}^2$). [BH₄⁻] ions (rigid body I): Center of the body (B1 atom) (0.3495(5), 0.0418(4), 0.546(1)). B-H distance: 1.227 Å. [NH₂NH₂] (rigid body II): NH₂ is defined as the rigid body and the geometry operation generates another half NH₂. Center of the body (N1 atom) (0.1544(5), 0.0956(4), 0.425(1)). N-H distance: 1.033 Å. [NH₂NH₂] (rigid body III): NH₂NH₂ is defined as the whole rigid body. Center of the body (N2 atom) (0.6478(4), 0.1923(5), 0.585(1)). Orientation angle about x , y , z -axis: $-2.3(4)^\circ$, $11.0(3)^\circ$, -32° . N-N distance: 1.463 Å, N-H distance: 1.036 Å. Mg at $2b$, $2c$, and $2d$ wychoff sites respectively. Refined lattice parameters are: $a=13.8385(8) \text{ \AA}$, $c=7.8284(8) \text{ \AA}$, and $V=1298.32(17)^\circ$. More crystallographic details can be found in the attached CIF file.

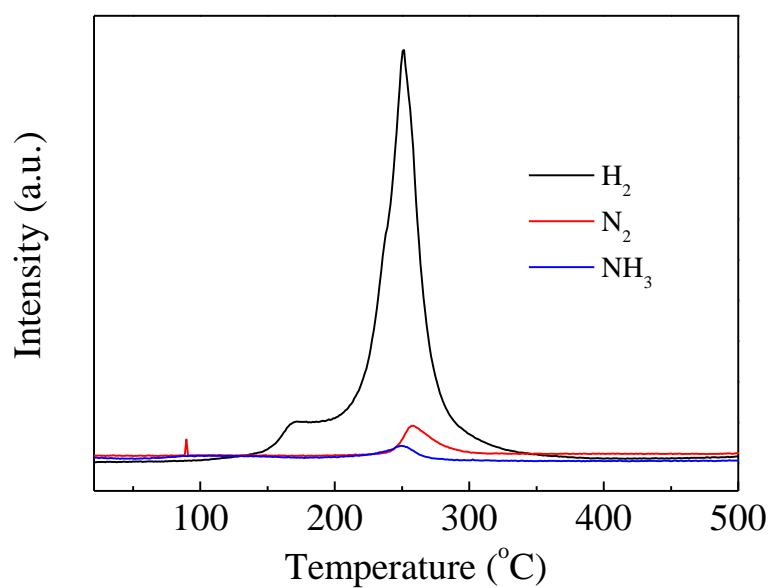


Figure S1 TPD-MS curves of $\text{Mg}(\text{BH}_4)_2 \cdot 3\text{N}_2\text{H}_4$.

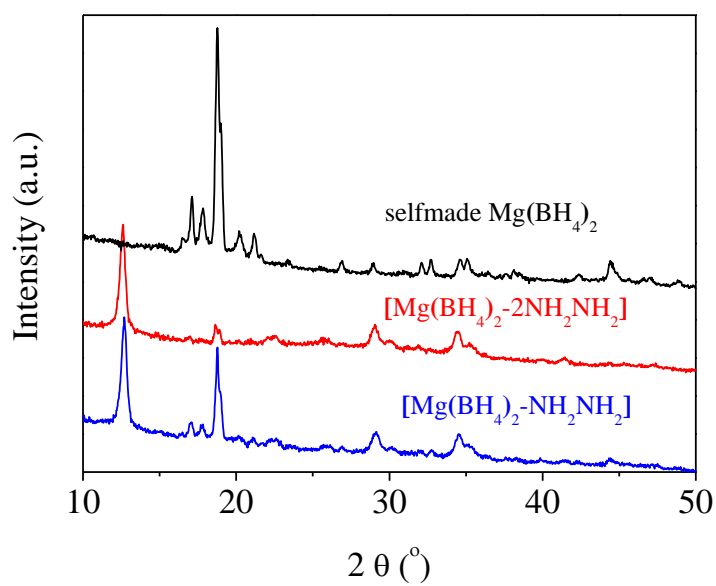


Figure S2 XRD patterns of $\text{Mg}(\text{BH}_4)_2$, $[\text{Mg}(\text{BH}_4)_2 \cdot 2\text{N}_2\text{H}_4]$ and $[\text{Mg}(\text{BH}_4)_2 \cdot \text{N}_2\text{H}_4]$.

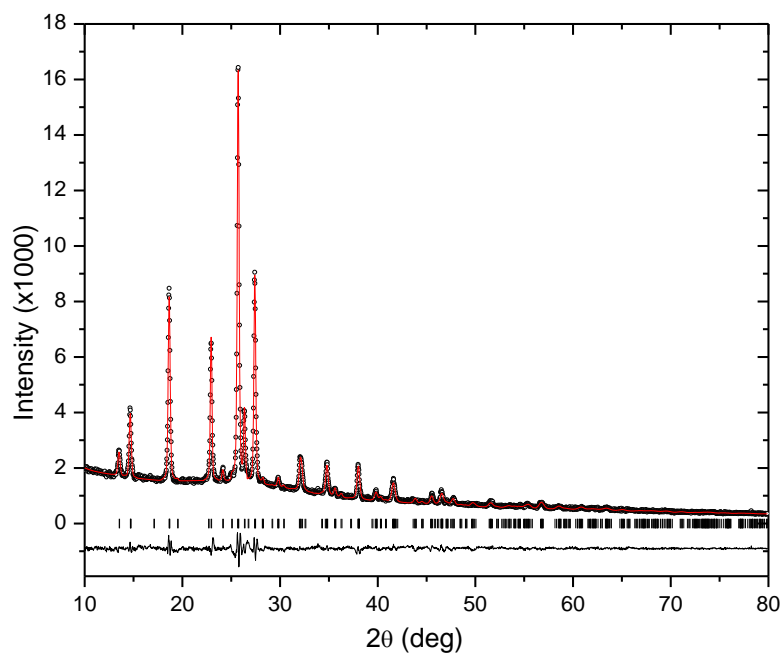


Figure S3 Experimental (circles), fitted (line), and difference (line below observed and calculated patterns) XRD profiles for $\text{LiBH}_4 \cdot 1/2\text{N}_2\text{H}_4$ at 298 K (CuK α radiation). Vertical bars indicate the calculated positions of Bragg peaks.

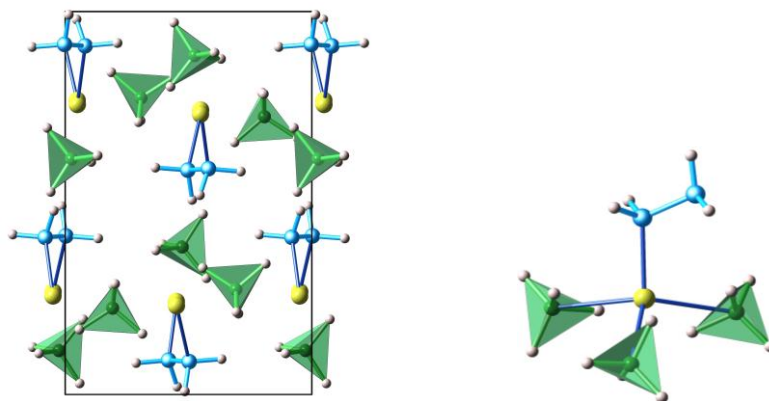


Figure S4 Crystal structure of $\text{LiBH}_4 \cdot 1/2\text{NH}_2\text{NH}_2$ (left) and close contacts around the Li^+ center in $\text{LiBH}_4 \cdot 1/2\text{NH}_2\text{NH}_2$ (right).

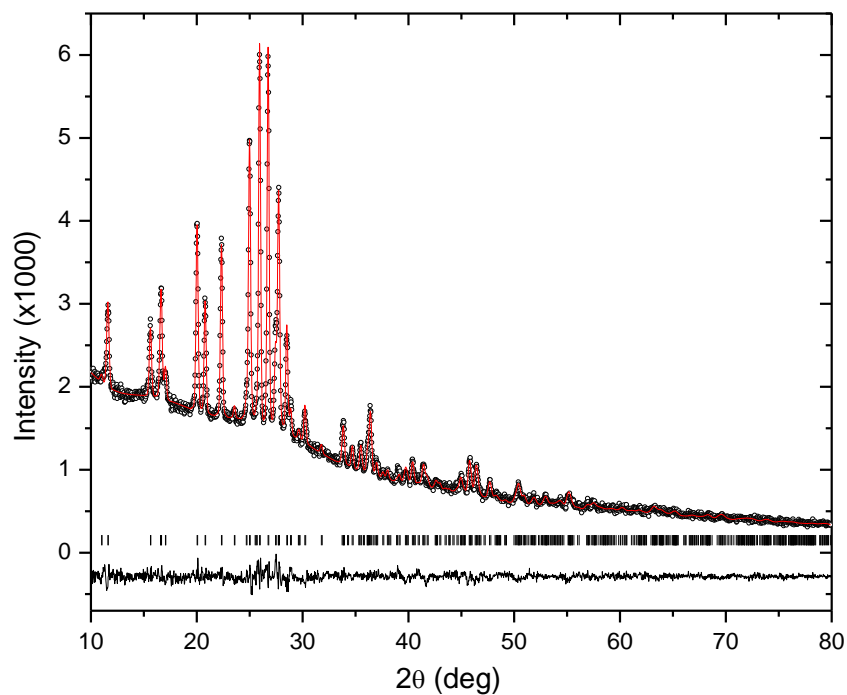


Figure S5 Experimental (circles), fitted (line), and difference (line below observed and calculated patterns) XRD profiles for $\text{LiBH}_4 \cdot 1/3\text{N}_2\text{H}_4$ at 298 K (CuK α radiation). Vertical bars indicate the calculated positions of Bragg peaks.

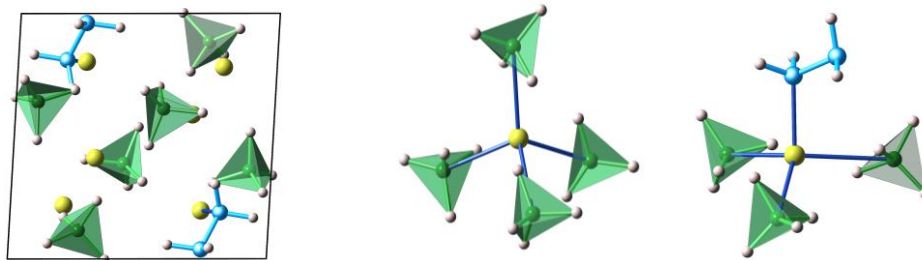


Figure S6 Crystal structure of $\text{LiBH}_4 \cdot 1/3\text{NH}_2\text{NH}_2$ (left) and two kinds of close contacts around the Li^+ center in $\text{LiBH}_4 \cdot 1/3\text{NH}_2\text{NH}_2$ (right).

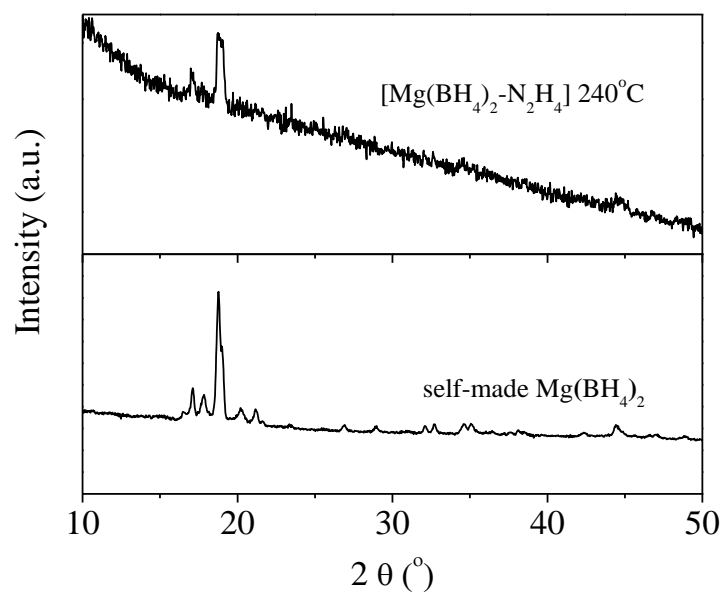


Figure S7 XRD patterns of post-dehydrogenated $[\text{Mg}(\text{BH}_4)_2\text{-N}_2\text{H}_4]$ at 240 °C compared with self-made $\text{Mg}(\text{BH}_4)_2$.

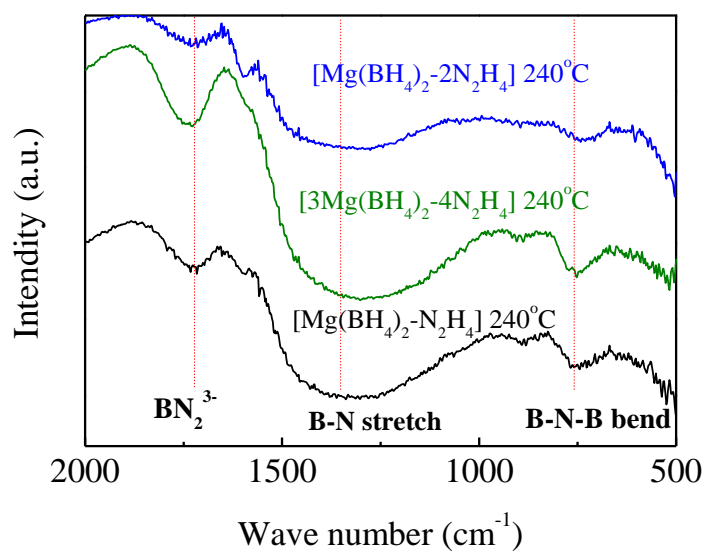


Figure S8 FT-IR spectra of post-decomposed $[\text{Mg}(\text{BH}_4)_2\text{-NH}_2\text{NH}_2]$, $[3\text{Mg}(\text{BH}_4)_2\text{-4NH}_2\text{NH}_2]$ and $[\text{Mg}(\text{BH}_4)_2\text{-2NH}_2\text{NH}_2]$ at 240 °C.

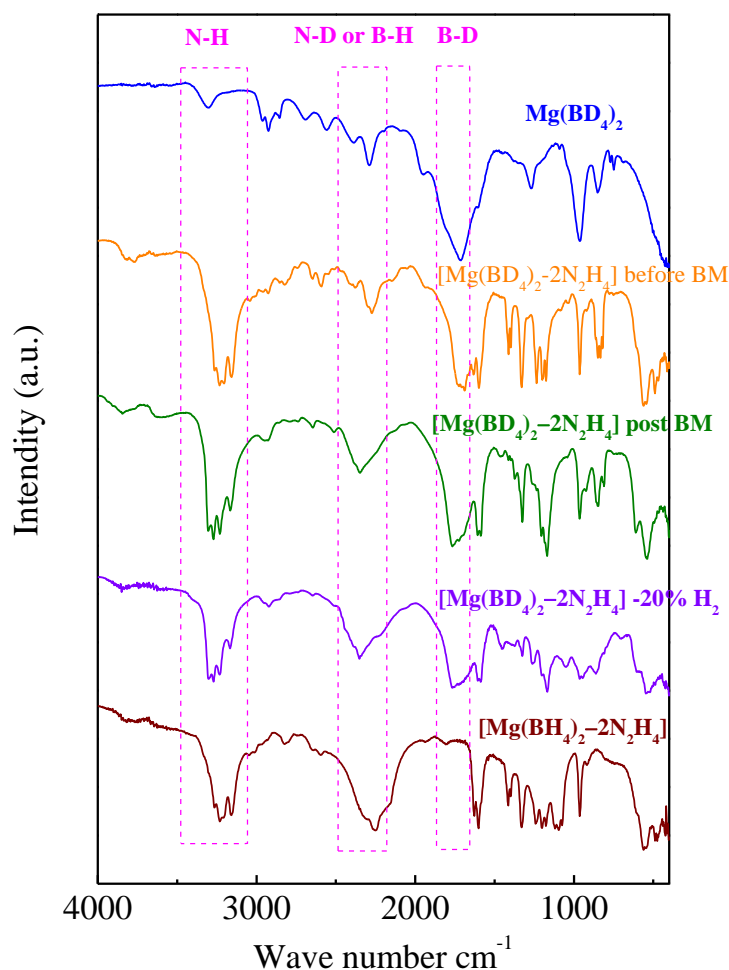


Figure S9 FT-IR spectra of $\text{Mg}(\text{BD}_4)_2$, $[\text{Mg}(\text{BH}_4)_2-2\text{NH}_2\text{NH}_2]$, $[\text{Mg}(\text{BD}_4)_2-2\text{NH}_2\text{NH}_2]$ before ball milling, $[\text{Mg}(\text{BD}_4)_2-2\text{NH}_2\text{NH}_2]$ post ball milling and $[\text{Mg}(\text{BD}_4)_2-2\text{NH}_2\text{NH}_2]$ post dehydrogenated 20% H_2 .

It can be seen that the sample $[\text{Mg}(\text{BD}_4)_2-2\text{NH}_2\text{NH}_2]$ before ball milling has strong B-D and N-H vibrations and a very weak B-H or N-D stretching at around 2290 cm^{-1} in FTIR from Figure S9. However, after ball milling for 2h, the frequency regions of B-H or N-D become stronger and broader, showing the exchange of hydrogen-deuterium. Additionally, the B-H and N-D vibrations regions grow even stronger when releasing 20% H_2 under heat treatment, further evidencing the occurrence of hydrogen-deuterium exchange during hydrogen desorption.

Reference:

1. Larson A. C., Von Dreele, R. B. *General Structure Analysis System*, Report LAUR 86-748. Los Alamos National Laboratory, NM, 1994.